catalysts

MDPI

Article

Synthesis of Oxygen Deficient TiO_2 for Improved Photocatalytic Efficiency in Solar Radiation

Kassim Olasunkanmi Badmus [1,*], Francois Wewers [1], Mohammed Al-Abri [2,3], Mohd Shahbaaz [4,5] and Leslie F. Petrik [6]

1 Chemistry Department, Cape Peninsula University of Technology, Bellville, Cape Town 7535, South Africa; WewersF@cput.ac.za
2 Nanotechnology Research Center, Sultan Qaboos University, Al-Khoud 123, Oman; alabri@squ.edu.om
3 Department of Petroleum and Chemical Engineering, College of Engineering, Sultan Qaboos University, Al-Khould 123, Oman
4 South African Medical Research Council, Bioinformatics Unit, South African National Bioinformatics Institute, University of the Western Cape, Private Bag X17, Bellville, Cape Town 7535, South Africa; mohammed.shahbaaz@gmail.com
5 Laboratory of Computational Modeling of Drugs, South Ural State University, 76 Lenin Prospekt, 454080 Chelyabinsk, Russia
6 Environmental and Nano Science, Chemistry Department, University of The Western Cape, Bellville, Cape Town 7535, South Africa; lpetrik@uwc.ac.za
* Correspondence: badmusk@cput.ac.za

Abstract: The photocatalytic activities of TiO_2 have been limited mainly to absorbing in the ultraviolet spectrum which accounts for only 5% of solar radiation. High energy band gap and electron recombination in TiO_2 nanoparticles are responsible for its limitations as a photocatalyst. An oxygen deficient surface can be artificially created on the titanium oxide by zero valent nano iron through the donation of its excess electrons. A visible light active TiO_2 nanoparticle was synthesized in the current investigation through simple chemical reduction using sodium boro-hydride. The physical and textural properties of the synthesized oxygen deficient TiO_2 photocatalyst was measured using scanning/ transmission electron microscopy while FTIR, XRD and nitrogen sorption methods (BET) were employed for its further characterizations. Photochemical decoloration of orange II sodium dye solution in the presence of the synthesized TiO_2 was measured using an UV spectrophotometer. The resulting oxygen deficient TiO_2 has a lower energy band-gap, smaller pore sizes, and enhanced photo-catalytic properties. The decoloration (88%) of orange (II) sodium salt solution (pH 2) under simulated solar light was possible at 20 min. This study highlights the effect of surface oxygen defects, crystal size and energy band-gap on the photo-catalytical property of TiO_2 nanoparticles as impacted by nano zero valent iron. It opens a new window in the exploitation of instability in the dopant ions for creation of a visible light active TiO_2 photocatalyst.

Keywords: nanoparticles; photo-catalyst; titanium (IV) oxide; energy band-gap; solar light

Citation: Badmus, K.O.; Wewers, F.; Al-Abri, M.; Shahbaaz, M.; Petrik, L.F. Synthesis of Oxygen Deficient TiO_2 for Improved Photocatalytic Efficiency in Solar Radiation. *Catalysts* **2021**, *11*, 904. https://doi.org/10.3390/catal11080904

Academic Editors: Paula Oulego and Ewa Kowalska

Received: 23 May 2021
Accepted: 23 June 2021
Published: 26 July 2021

1. Introduction

The oxides of semiconductors are capable of absorbing a substantial quantity of (UV) radiation from a sunlight source and thus generate electron/hole pairs. This forms the basis of their utilization in photocatalysis and several other applications [1]. The generated electrons are capable of using the available excess energy to gain promotion (excitation) from the valence band (VB) to the conduction band (CB) and therefore leave behind positive holes. These holes are capable of breaking down water molecules into hydrogen and hydroxyl radicals as the electrons react with oxygen to produce the superoxide anion (O^{-2}) [2,3]. Thereafter, both radicals and super-oxides react with persistent chemical or biological contaminants to generate more biodegradable end products [4]. Under solar radiation, the degradation of water contaminants is possible at room temperature and

atmospheric pressure when an appropriate semiconductor photocatalyst is applied. The degradation depends on the physicochemical properties of the pollutants as well as the surface area/functionality of the photocatalysts, type of pollutant, its concentration and the solution pH [5].

A high conduction band level in most semi-conductors constitutes a great limitation to generation of electron-hole pairs and, consequently, application in photocatalysis [6]. Meanwhile, superior capability for utilization of solar light and high stability towards photo-corrosion are the advantages of TiO_2 over other nonmetal oxides as a photocatalyst [7]. The associated high energy band gaps and agglomeration of TiO_2 severely limit its application as a photocatalyst in water treatment [4]. Sustainability of photo-degradation processes can be achieved by the synthesis of TiO_2 with enhanced capacity for solar-light harvesting through improvements in the documented disadvantages [8,9]. Common techniques such as modification by organic materials, semi-conductor coupling and metal doping can be employed to create surface defects on TiO_2 and consequently reduce the energy band gap and prevent the agglomeration [10].

Recent investigations have shown that doping of TiO_2 with alien ions such as rare-earth metals, transition metals or nonmetals can substantially improve its photocatalytic property [11]. Introduction of dopant ions ensures the reduction of the band gap through the modification of the electronic structure. Consequently, a finite amount of electrons can reach the conduction band and causes reduction in the massive recombination of the charge carriers [12]. There is a capacity for reduction of trapped electron density and in charge recombination through induced oxygen vacancies on the surface of TiO_2 [13]. The relationship between oxygen vacancies and photocatalytic activities of the semiconductor is well documented [10,14]. Metals with partially filled d-orbitals such as transition metals can cause acceleration in electron–hole generation because of their similarity in electronic configuration to TiO_2 [15,16]. They are capable of creating a localized electronic state in the valence band and conduction band of TiO_2 [17,18]. However, the electronegativity and variable oxidation states in transition metals can hinder their application as a dopant in the optimization of the photo-catalytic property of TiO_2 [19].

Meanwhile, non-metals such as sulfur, carbon and nitrogen can also serve as dopants through their substitution for oxygen atoms in TiO_2 [20]. The p-orbitals in the non-metal can narrow the energy band gap by introducing new electronic states above the valence band. Besides, multiple metals or metal–nonmetal co-doping have been successfully investigated and reported for their lower band-gaps in comparison to a single metal or non-metal [21]. It is known that the possibilities of forming donor–acceptor pairs in metal–nonmetal co-dopant leads to electronically higher energy and subsequent enhanced activity in the visible electromagnetic regions [22].

Just like metal–nonmetal dopants, an electronically unstable element can cause oxygen deficiencies on the surface of TiO_2 as it attains partial stability [23]. The theoretical view of the current investigation was governed by the possibility of creating donor–acceptor pairs on the surface of an intrinsic TiO_2 to achieve optimum reduced band-gap as well as to prevent recombination of the charge carriers. The instability of zero valent nano iron (nZVI) was reported in one of our previous publications [24]. nZVI could produce the required oxygen vacant surface for absorption in the visible spectrum of electromagnetic radiation by the TiO_2. The associated excess electrons on nZVI can be transferred to the surface oxygen electron of the TiO_2. This may result in the delocalization of the surface electron in TiO_2 and cause significant increment in electron density. The impact of zero valent nano iron on the photocatalytic properties of the produced TiO_2 will be studied in the current investigation.

2. Results and Discussion

The electronic configurations for TiO_2 (unit cell) and Titanium doped nZVI (Yb, 2 × 2 × 1 supercell) are presented in Figure 1A,B. The red, gray, and purple spheres represent oxygen, titanium, and iron atoms, respectively.

(**A**)

(**B**)

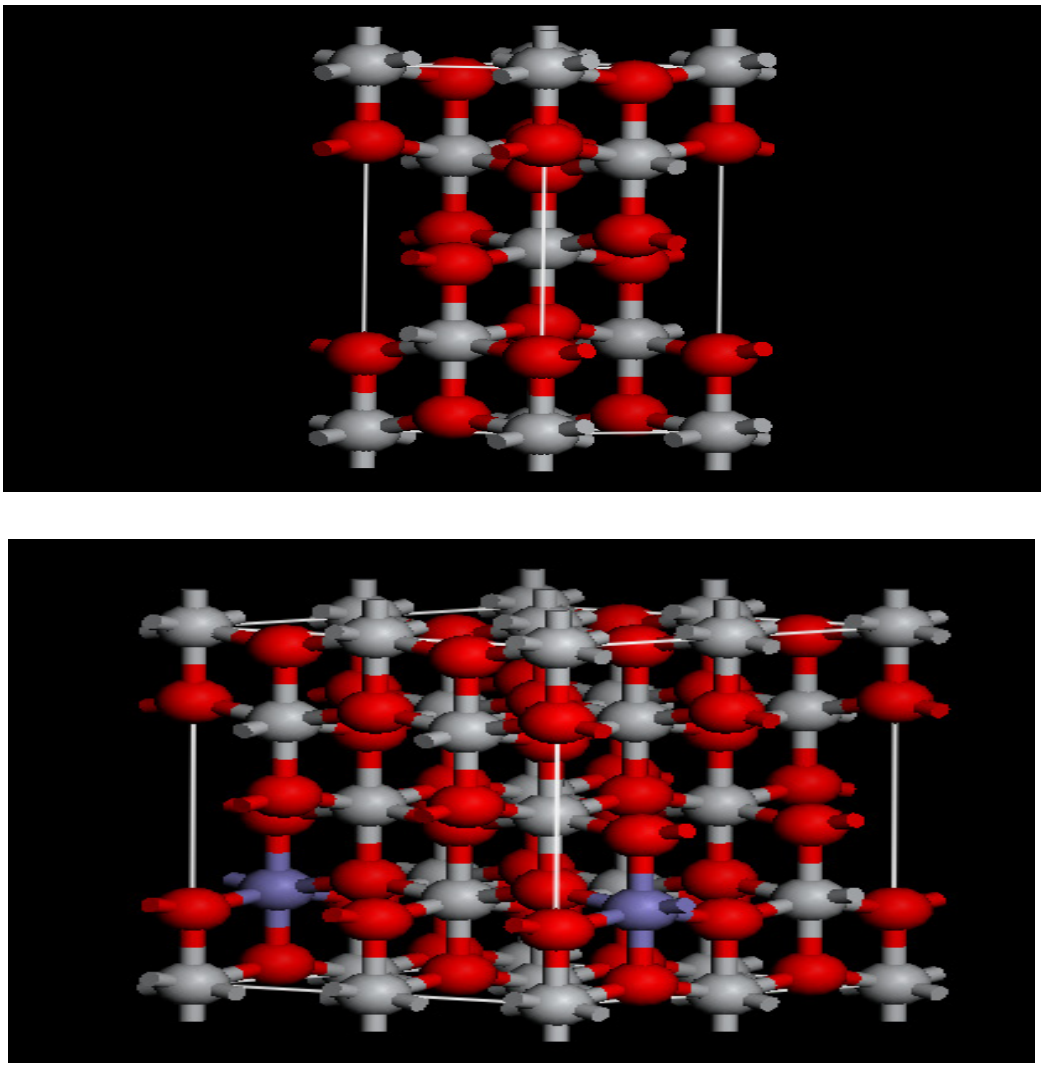

Figure 1. (**A**) The unit cell of Reference TiO_2 and (**B**) oxygen deficient TiO_2 supercell.

The calculated band structure of a unit cell of anatase TiO_2 displays a band gap of 2.242 eV as calculated from computational simulation. When the doped supercell structure with 2 × 2 × 1 cell containing 48-atom of anatase TiO_2 was used, and a Ti atom in the vicinity of the center of the supercell was replaced by a nZVI atom, the calculated band gap of zero valent nano iron-doped TiO_2 (TD) was 2.083 eV. The injection of electron surplus nZVI increases the number of electrons on the titanium atoms and its conversion from Ti4+ to a lower oxidation state (Ti3+). The induced structural disorder in zero valent nano iron-doped TiO_2 (TD) was primarily responsible for the lower energy band gap [25].

2.1. Absorption of Zero Valent Nano Iron-Doped TiO_2 under Electromagnetic Spectrum

The UV spectra of a reference TiO_2 (T_R) was compared to that of the synthesized oxygen deficient TiO_2 (T_D) in order to investigate the change in optical absorption characteristic. Additionally, the band gap of T_R and T_D were calculated from the UV-Vis spectra.

As shown in Figure 2, the light absorption edges of reference T_R and that of T_D were approximately 321 nm and 334 nm, respectively. Redshift to the visible region (longer wavelength) in UV absorption of T_D is the direct effect of nZVI on the surface of TiO_2. This is a clear indication of an enhanced solar absorption in T_D [26,27]. An alternative energy level was created as a consequence of interactions among the electrons of titanium oxide and the nZVI. Consequently, a stronger absorbance yield was observed in the synthesized oxygen deficient TiO_2 (T_D) in relative to the reference TiO_2 (T_R). The implication of this

change in visible light activity of the T_D on its energy band gab variation can be further investigated using a Tauc's plot (1).

$$(\alpha h\nu)^{1/n} = C(h\nu - E_g) \quad (1)$$

where: α is the absorption coefficient, h is Planck's constant, ν is frequency ($\nu = c/\lambda$, c is the light speed, λ is the wavelength), $n = \frac{1}{2}$ and 2 for direct and indirect optical band gap, respectively, C is proportionality constant and E_g is band gap.

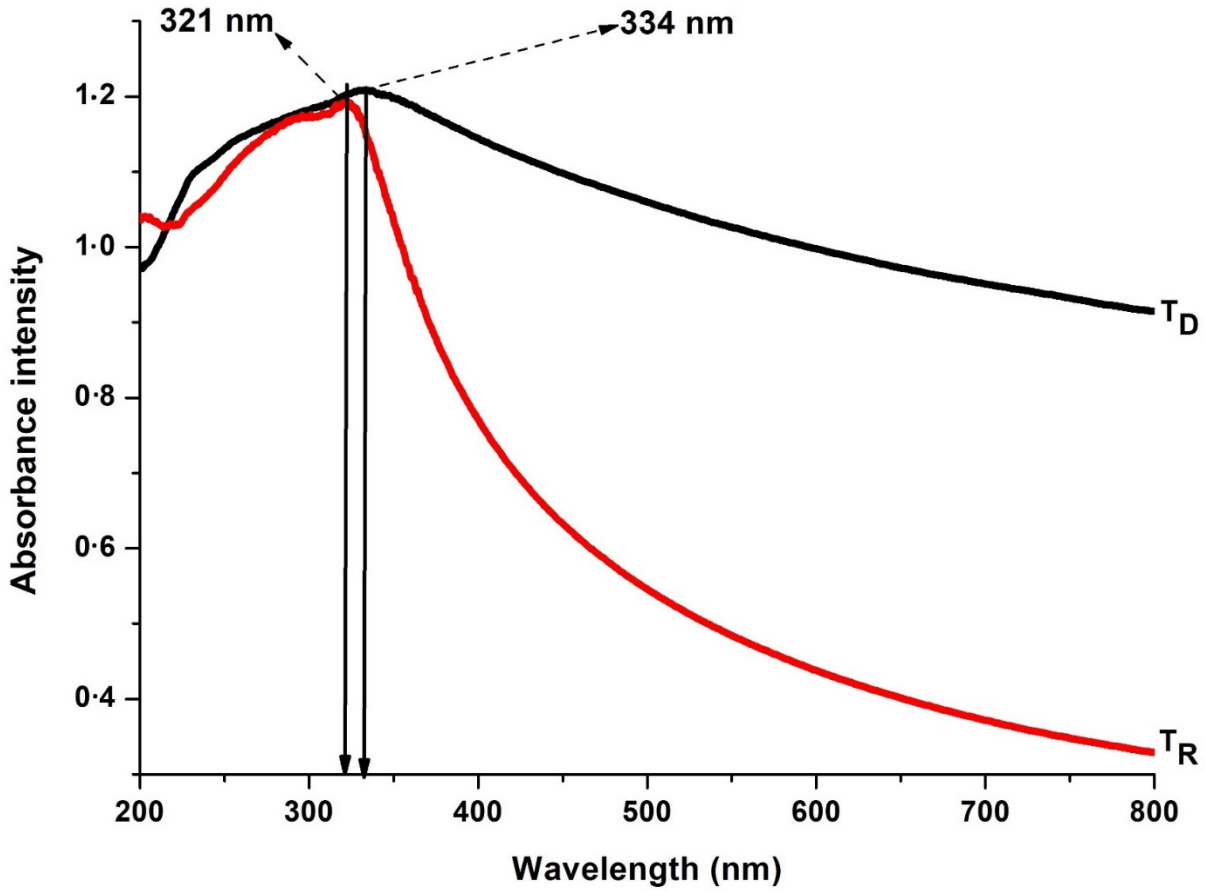

Figure 2. UV spectrophotometer analysis of reference Titanium oxide (T_R) and Titanium doped nZVI (T_D).

The synthesized oxygen deficient TiO_2, (T_D) resulted in a lower energy band gap (2.24 eV) in comparison with the reference TiO_2, (T_R) (2.95 eV), Figure 3.

The band gap variation of 0.71 eV obtained between the T_D and T_R is as a result of the improvement in electrical conductivity and mobility of charge carriers in the oxygen deficient TiO_2 (T_D). This can lead to a reduction of bulk recombination in the photo generated electron-hole pairs [28]. The higher transmittance intensity as observed on the FT-IR spectra of synthesized T_D in comparison to that of T_R is an indication of an enhanced infrared activity in the synthesized oxygen deficient TiO_2 (Figure 4). The peak at 1040 due to Ti–O stretching vibration was only detected in the FT-IR spectra of T_D. Likewise, the peculiar O–Ti–O lattice bonding of the anatase TiO_2 was pronounced in the FT-IR spectrum of the T_D at 1382 cm^{-1} [29] and not the FT-IR of T_R. However, the FT-IR peak at 1643 cm^{-1} is an indication of ferric oxyhydroxide (FeOOH) caused by oxidation of surface nZVI [30]. Likewise, FT-IR peak at 3322 cm^{-1} is related to the O–H bending vibrations spectra of TiO_2 (T_D) as a result of added hydroxyl groups due to water absorption on the nZVI surfaces

as reported by Mragui et al. (2019) [30]. Apparently, the FT–IR result as presented in the current investigation showed lack of infrared activity in the reference TiO_2 (T_R) compared to the synthesized oxygen deficient TiO_2 (T_D).

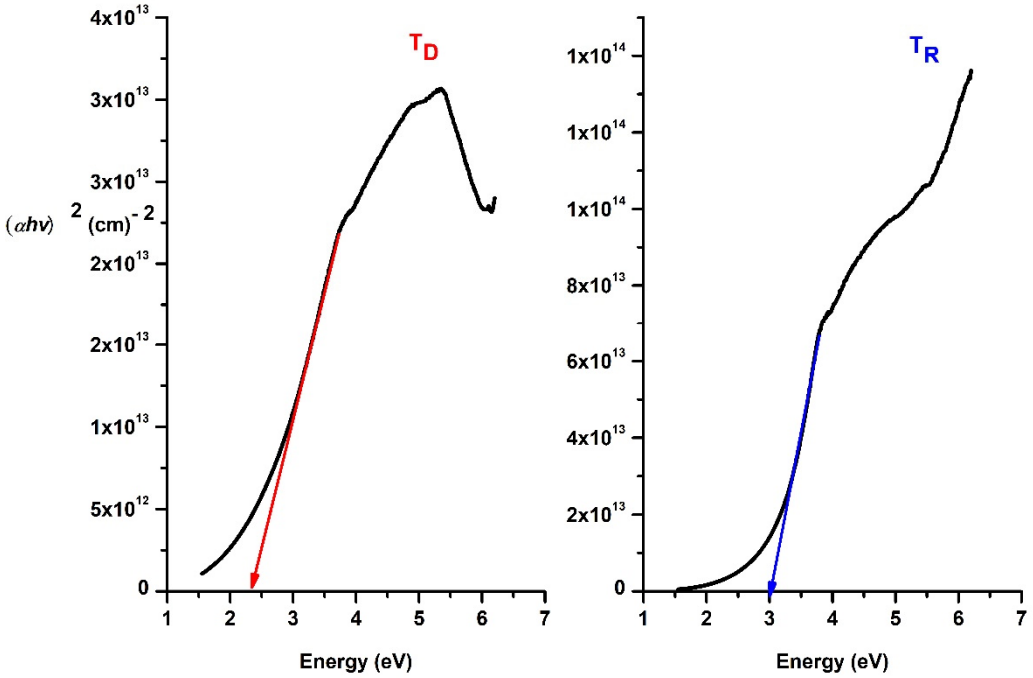

Figure 3. TAUC's plot of reference for Titanium oxide (T_R) and Oxygen deficient Titanium (T_D) showing the energy band gaps.

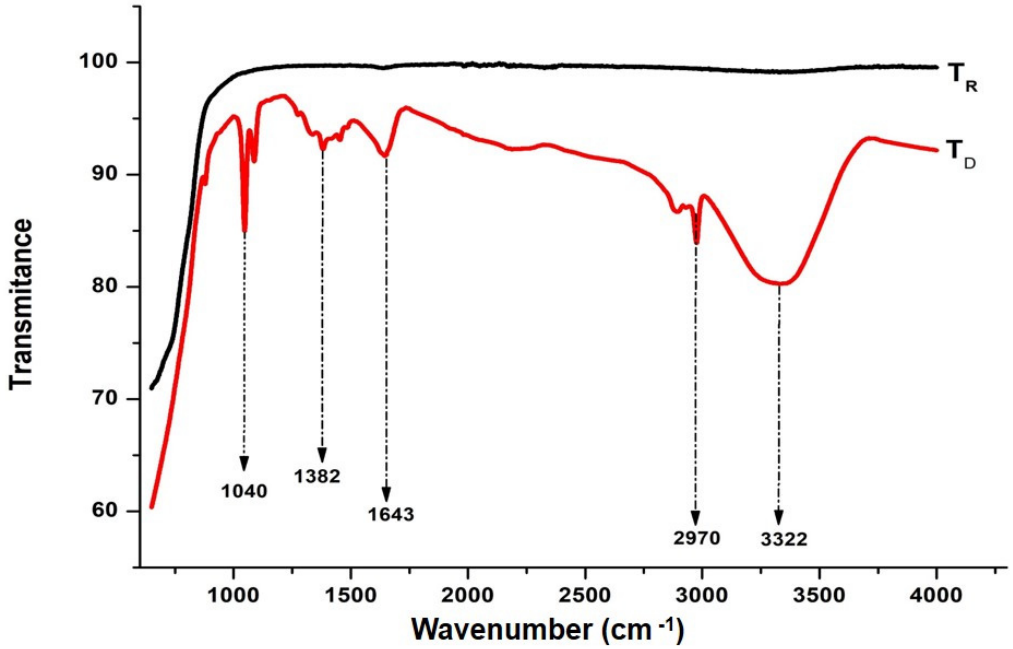

Figure 4. FT–IR analysis of reference Titanium oxide (T_R) and Titanium doped nZVI (T_D).

The adsorbed OH ions have a propensity for trapping charge carriers and produce reactive hydroxyl (OH) radicals [31]. The produced OH radicals are capable of attacking the active sites of stable compounds or initiating nonspecific degradation of pollutant molecules [32]. It can be confirmed through the current FT–IR results that the synthesized

TiO_2 is oxygen deficient and highly hydrogenated. These characteristics can result in a state of strong localization between the valency band and conduction bands [33,34]. Further studies of the interaction of nZVI on TiO_2 can be carried out by assessing the change in crystallite sizes of the titanium (IV) oxide.

2.2. Morphology, Surface Area and Size Distributions

Diffraction patterns of reference and the synthesized TiO_2 (T_R and T_D) were as presented in Figure 5. The XRD of T_R and T_D nanoparticles gave 2 Theta (2θ) peaks at 20.33°, 22.47°, 32.88°, 43.09°, 49.12°, 50.15°, 57.78°, 63.97°, 65.35° and, 70.15°, corresponding to crystal planes of (101), (110), (004), (200), (105), (211), (204), (116), (220) and (215) for crystalline titanium oxide nanoparticles.

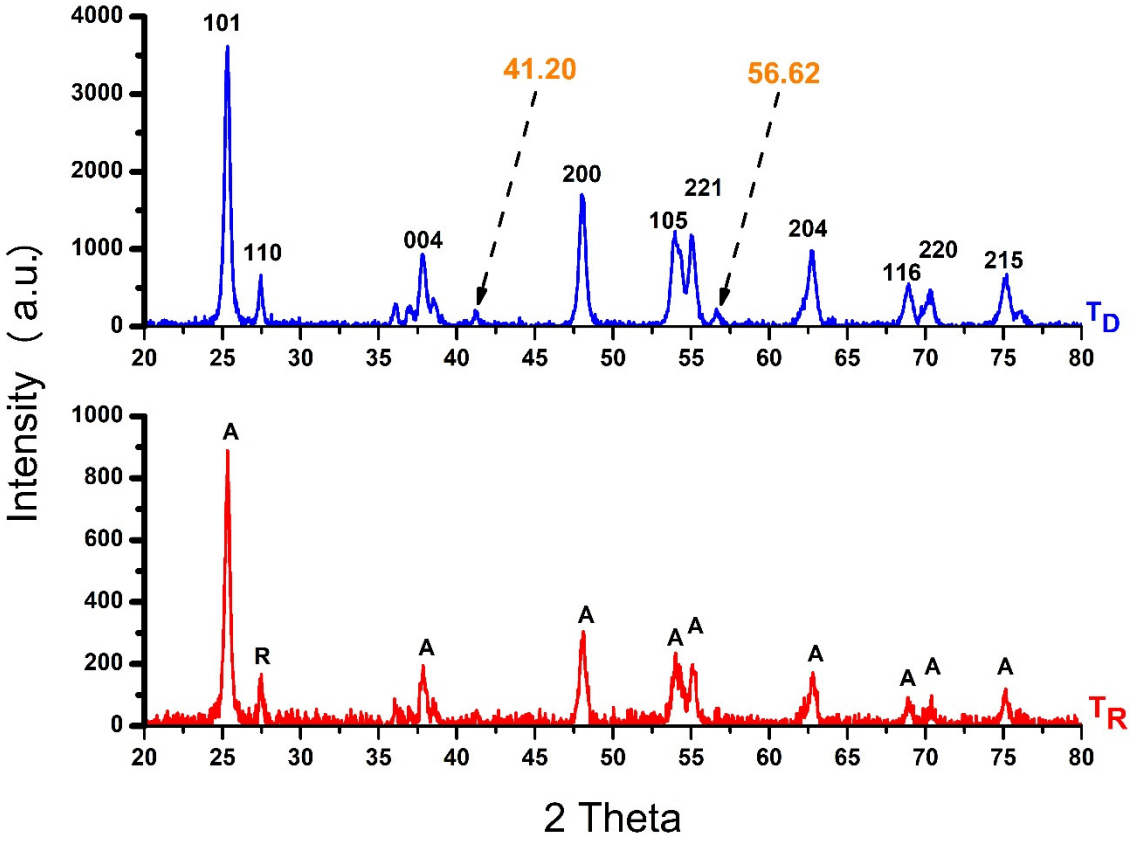

Figure 5. XRD analysis of reference Titanium oxide (T_R) and Titanium doped nZVI (T_D).

This result is in agreement with the standard XRD pattern (JCPDS-21-1272) and the peaks can be indexed as anatase phases of TiO_2 (in the majority of cases) with body center tetragonal shape [35]. All orientations due to anatase phases of TiO_2 were observed in both samples with higher intensity on T_D which means higher crystallinity [36]. The observed 2theta peaks at 41.20 and 56.62 were attributed to traces of elemental iron present as nZVI particles [30,37,38]. The nZVI particles may be responsible for oxygen deficiency on titanium surfaces leading to an improved crystallinity in TiO_2 nanoparticle [39]. The crystallite sizes of the synthesized and reference TiO_2 nanoparticles were obtained by using Debye-Scherrer's Equation (2).

$$D = \frac{K\lambda}{(\beta\, COS\theta)} \quad (2)$$

D is the crystal size while the wavelength of the X-ray radiation λ = 0.15406 nm for CuKα.

K = 0.9 and β (FWHM radians) is the line width at half-maximum height and θ the peak position (radian). According to Debye-Scherrer's formula, the obtained crystallite sizes for TiO_2 nanoparticles T_R and T_D were 17.91 nm and 15.31 nm, respectively. The derived crystallite sizes reflect the surface reductions and bulk defects in the synthesized zero valent nano iron-doped TiO_2 [40].

Transmission Electron Microscope (TEM) and Scanning Electron Microscope (SEM) images were used respectively to define the morphologies, surface areas and sizes of TiO_2 nanoparticles T_R and T_D (Figure 6) The average sizes and distributions in the TiO_2 nanoparticles were determined using image J, software (NIH, Media Cybernetics Inc. Rockville, MD, USA) to process the derived images from TEM analysis. The average size with high frequency was between 16–20 nm for TiO_2 nanoparticles T_R and T_D. SEM micrographs show that the synthesized TiO_2 nanoparticles (T_D) were slightly smaller than the reference TiO_2 (T_R) nanoparticles on average. The SAED ring pattern displayed d-spacing values and hkl planes with a characteristic tetragonal anatase phase of TiO_2 nanoparticles, which was equally reported for TiO_2 nanoparticle synthesized by Hengerer et al. (2000) [41]. A remarkable decrease in the crystal sizes of TiO_2 nanoparticle T_D relative to the reference TiO_2 nanoparticle T_R was noted in the histogram, as seen in Figure 6A,B. This has been reported for the provision of the corresponding positive effect on the dispersion and prevention of agglomeration in the nanoparticles [42].

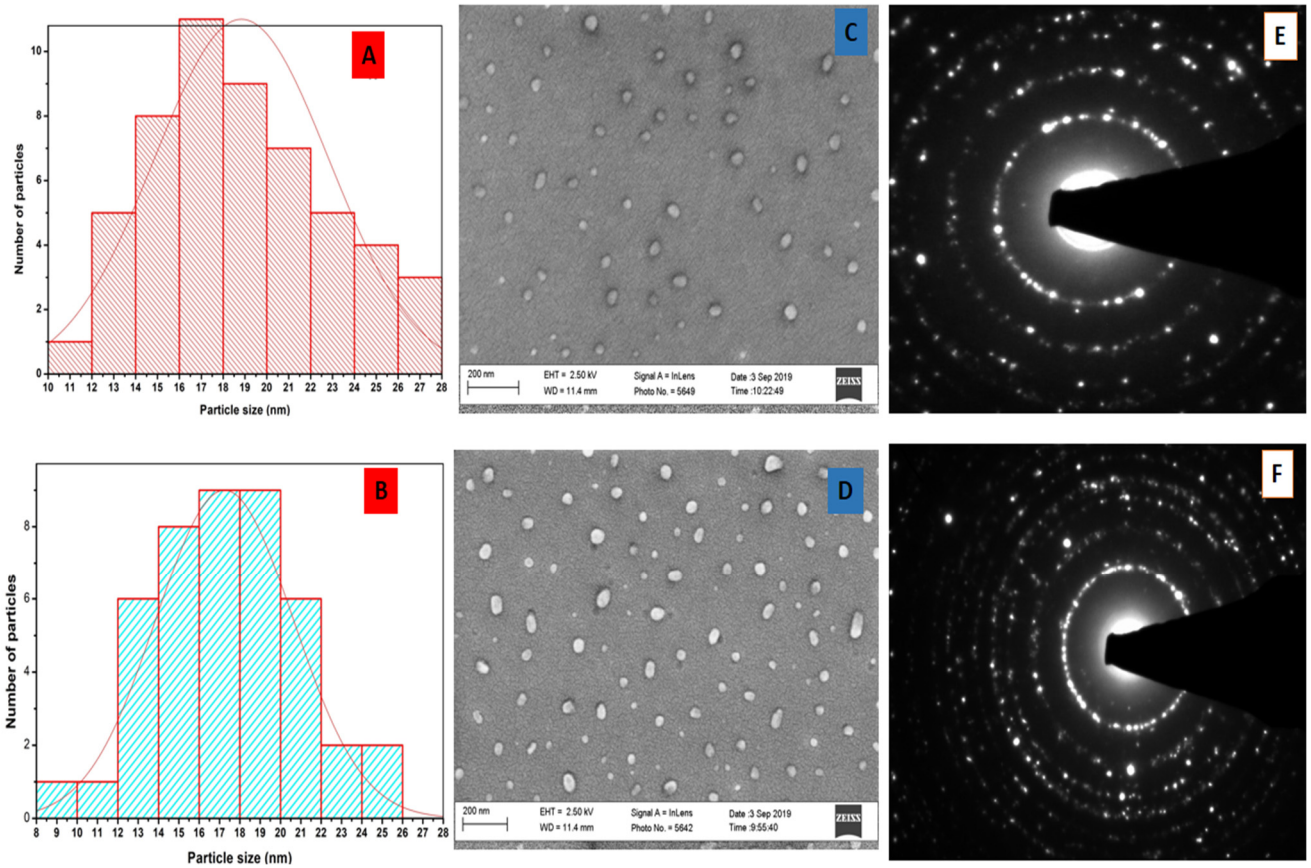

Figure 6. TEM histogram (**A**,**B**); images (**C**,**D**) and SAED (**E**,**F**) of reference T_R and T_D, respectively.

The SEM-EDS elemental analysis of TiO_2 nanoparticles as presented in Figure 7 confirmed the polycrystallinity nature of the reference (T_R) and synthesized TiO_2 nanoparticles (T_D).

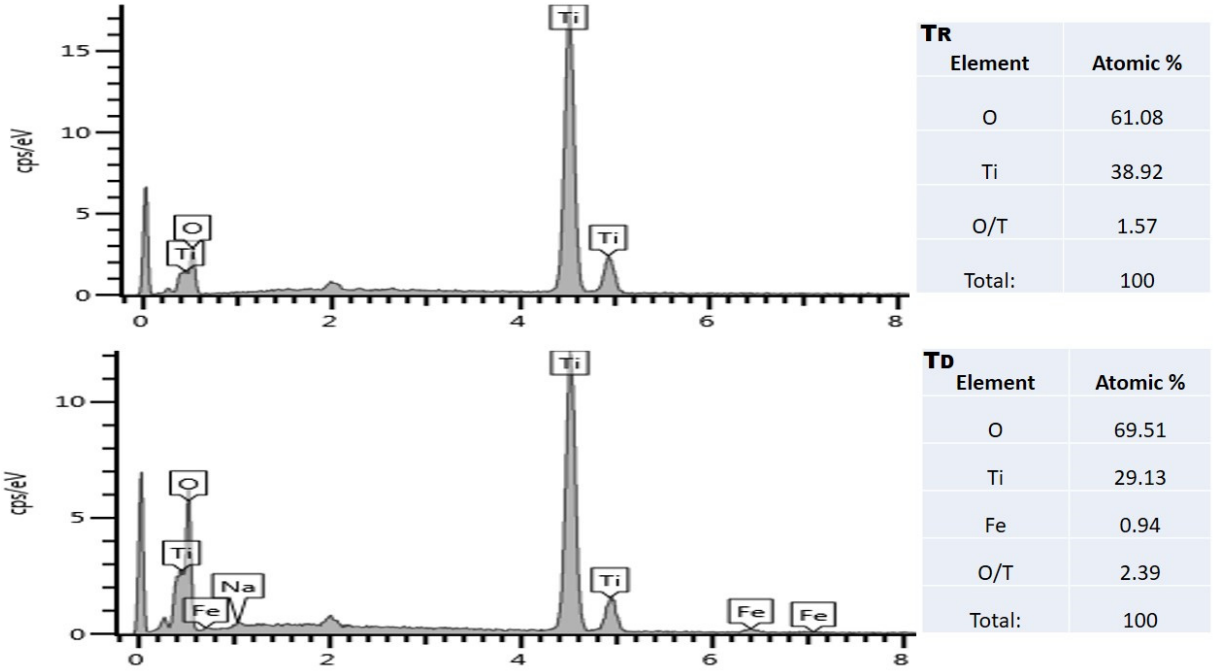

Figure 7. SEM-EDS of reference TiO_2 and synthesized zero valent nano iron-doped TiO_2.

Major identified elements were oxygen (O), titanium and iron (Fe) while traces of sodium (Na) were confirmed on SEM-EDS of T_D as impurities. The oxygen/ titanium ratio (O/T) in the EDS was determined to confirm the oxygen deficient impact of the synthesized TiO_2 nanoparticles (T_D). It was discovered that T_D has a higher oxygen content (O/T = 2.39) in comparison with T_R (O/T = 1.57). The observed higher oxygen content in the synthesized oxygen deficient TiO_2 (T_D) was a resultant effect of the oxidized nZVI on the TiO_2 nanoparticle. The oxygen deficiency was created when iron shared its excess electron with the titanium oxide nanoparticles. Recently, Ti^{3+} spice production has been reported when the excess electron on nZVI migrated into the empty spaces in titanium ions [7,43].

The adsorption–desorption isotherms of the reference and synthesized TiO_2 (T_R and T_D) exhibit type IV isotherm with a hysteresis loop at a relative pressure in the range 0.8–1.0 (Figure 8). This is characterized by capillary condensation, indicating mesopores solids with weak interaction features [44]. Detailed observation of isotherms revealed a narrower desorption in the T_D compared to T_R. A reduction of pore volume of the sample T_D compared to T_R (from 0.19 to 0.18 cm^3/g) as presented in Table 1, indicated the withdrawal of oxygen from TiO_2 nanoparticles. This led to an enlargement of pore sizes as observed in the BET pore diameter of T_D presented in the current investigation. The reduction in porosity of T_D leads to a corresponding reduction in the BET surface area of the synthesized TiO_2 samples (T_D). The reduction in the BET surface area of the synthesized TiO_2 nanoparticles (T_D) can prevent electron recombination through the alteration in migration path of electron charges to the surface of the photocatalyst.

Table 1. BET surface area (S_{BET}), Pore volumes, Pore sizes (Pore diameter) Energy bandgap (E_g), XRD sizes (d_{XRD}) of the reference TiO_2 and synthesized TiO_2.

TiO_2 Photocatalyst	S_{BET} (m^2/g)	Pore Volume (cm^3/g)	Pore Size (A^0)
T_R	53.78	0.1897	137.6
T_D	44.62	0.1799	158.1

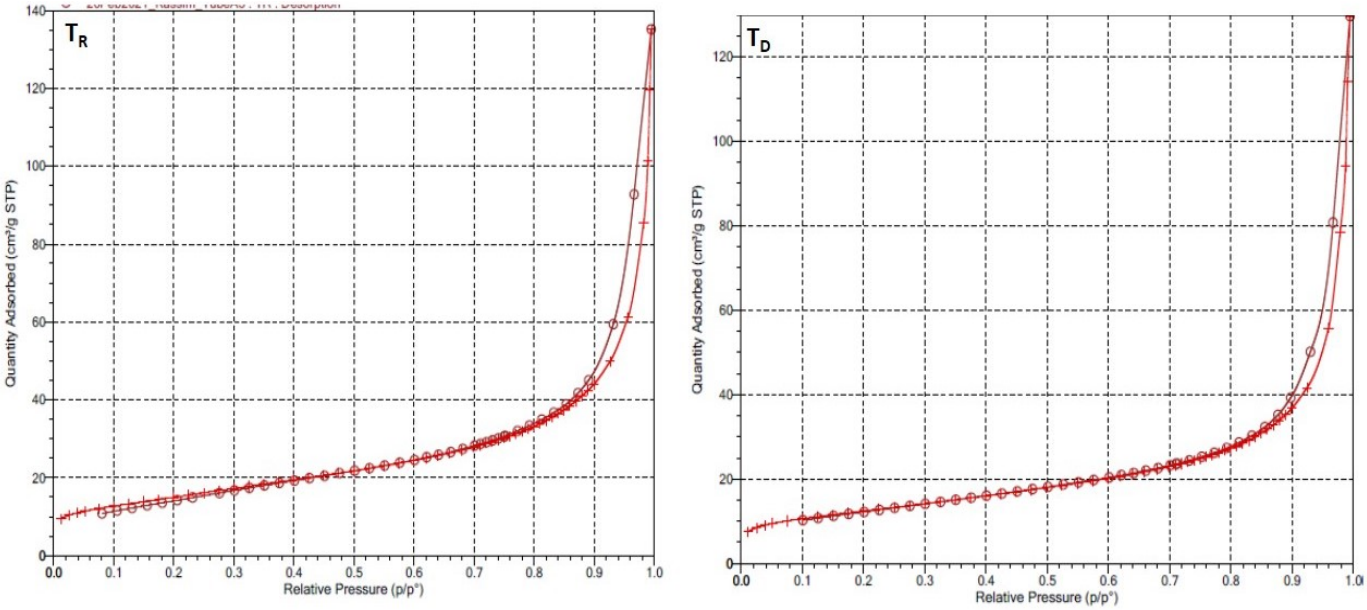

Figure 8. Nitrogen adsorption–desorption isotherm for the reference Titanium oxide (T_R) and oxygen deficient Titanium oxide nanoparticles (T_D).

2.3. Photo-Catalytic Application of the Synthesized Titanium Oxide Nanoparticle

The % decoloration of orange II sodium salt during photocatalysis using solar simulator in the presence of the T_R and T_D were compared (Figure 9). Orange II sodium salt was used in the current investigation because of its stability, structural resemblance to common organic pollutant and the ease of monitoring the decoloration using an Ultraviolent Spectro-photometer instrument. It was observed that T_D had a higher activity as a photocatalyst in the visible region under solar light irradiation compared to the T_R. The lower extent (%) of orange II sodium salt decoloration at dosage of 50 mg may be as a result of solar light path blockage by the high concentration of photocatalyst (500 mg/L).

The photo-catalytical decoloration of orange II sodium salt solution can also be influenced by its pH (Figure 10). This was tested by applying the optimum number of titanium oxide nanoparticles (T_R or T_D at 250 mg/L) in the decoloration of orange II sodium salt under the influence of simulated solar light. It was observed that the rate of decoloration increased as the solution became more acidic with the optimum decoloration achieved at pH 2 for both the reference TiO_2 (T_R) and synthesized oxygen deficient TiO_2 nanoparticles (T_D).

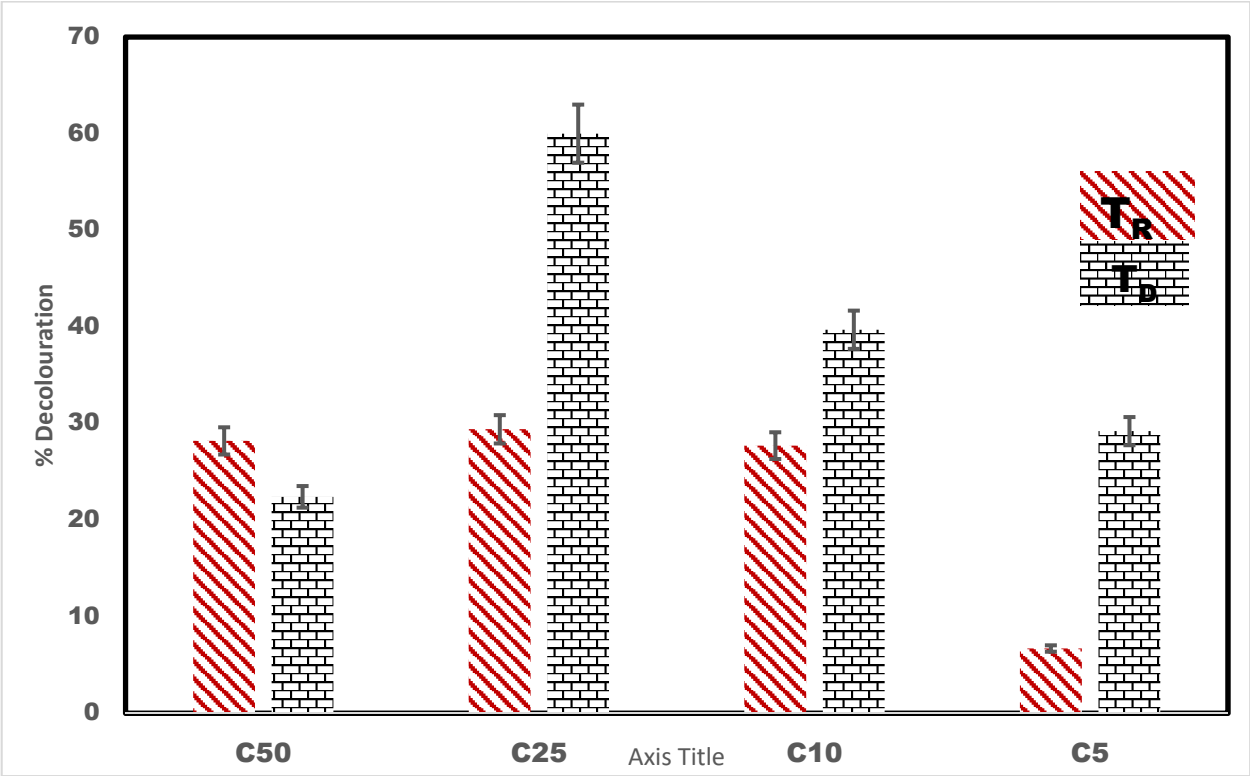

Figure 9. % Decoloration of orange II sodium salt (10 mg/L) by T_R and T_D at 50 mg/L (C5), 100 mg/L (C10), 250 mg /L (C25) and 500 mg/L (C50) dosage of titanium oxide nanoparticles.

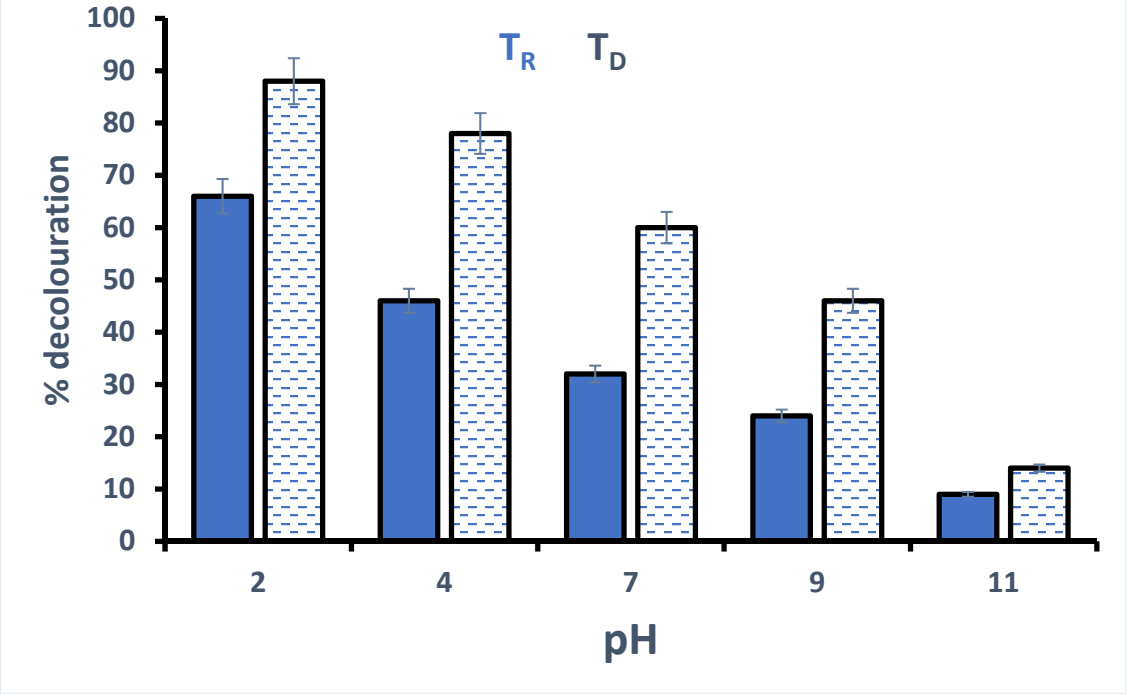

Figure 10. *Cont.*

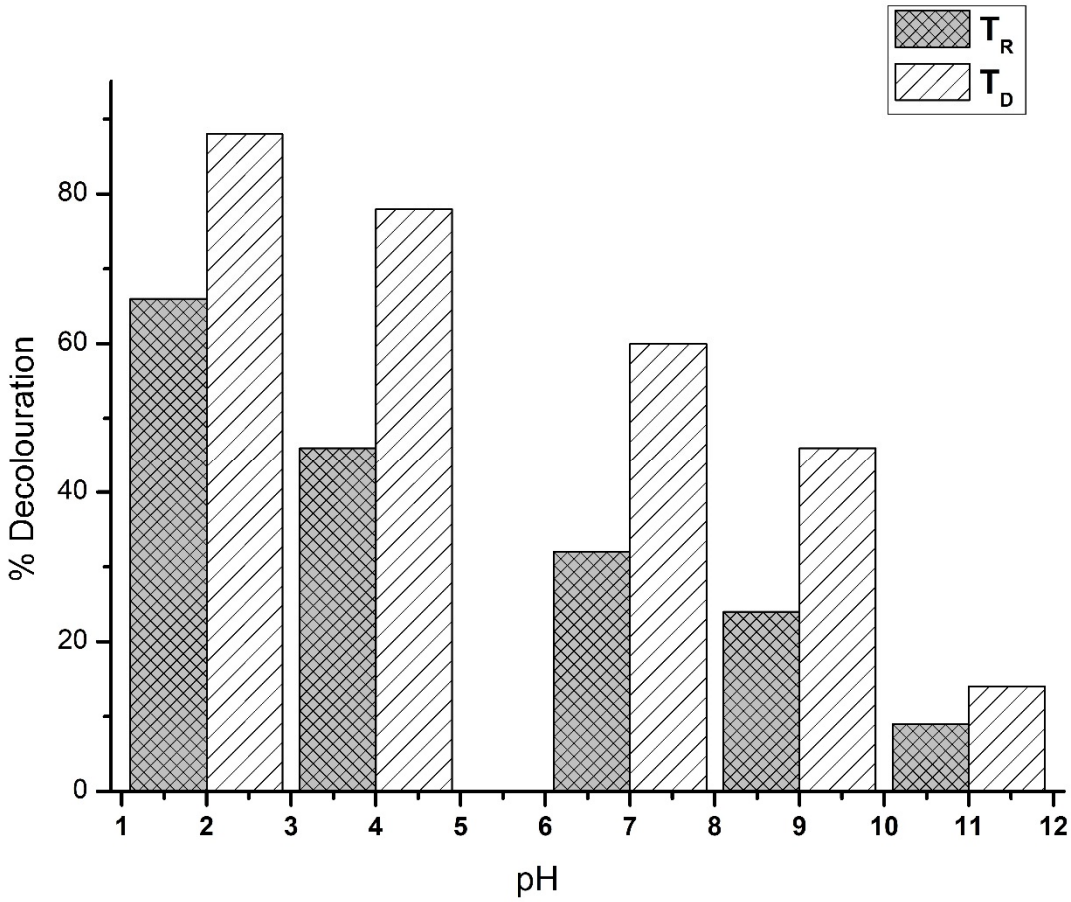

Figure 10. % Decoloration of orange II sodium salt solution under the photocatalytic effect of TiO_2 nanoparticles T_R and oxygen deficient TiO_2 nanoparticles T_D at solution pH (pH 2, pH 4, pH 7, pH 10 and pH 11).

3. Materials and Methods

3.1. Materials

Titanium (iv) oxide nano-powder (99.5%), Orange II sodium salt (analytical standard) with structural resemblance to common pharmaceutical, Hydrochloric acid (37%) and Absolute ethanol (99.9%) were purchased from Sigma-Aldrich Co. Ltd. (Buchs, Switzaland), and anhydrous $FeCl_3$ (99.99%) and sodium borohydride powder (98%) were purchased from Saar Chem Pvt, Ltd (Mumbai, India). Sodium hydroxide pellets (97%) were purchased from Merck Chemicals (Pty) Ltd (Germiston, South Africa). All analytical grade chemicals were used without further purification during the experiment process.

3.2. Preparation Method

The oxygen deficient TiO_2 was prepared by dissolving 500 mg of nano-powder TiO_2 and 20 mg $FeCl_3.6H_2O$ in 50 mL deionized water (as presented in Figure 11). The solution was poured into a three necked round bottom flask and stirred (magnetically) for 30 min in an inert (nitrogen) environment (Figure 1). The prepared solution was purged with nitrogen to ensure the removal of dissolved oxygen. A 20 mL sodium borohydride solution (5000 mg/L) was added to the contents of the (three necked) round bottom flask and stirred for 30 min for the production of oxygen deficient TiO_2 photocatalyst. Ethanol (99%) was added to prevent reversed oxidation of the produced nanoparticles. The solution was subsequently washed through pressure filtration using filter paper (0.45 micron) connected to a Bucher flask vacuum filter system and ethanol was repeatedly added to ensure thorough washing.

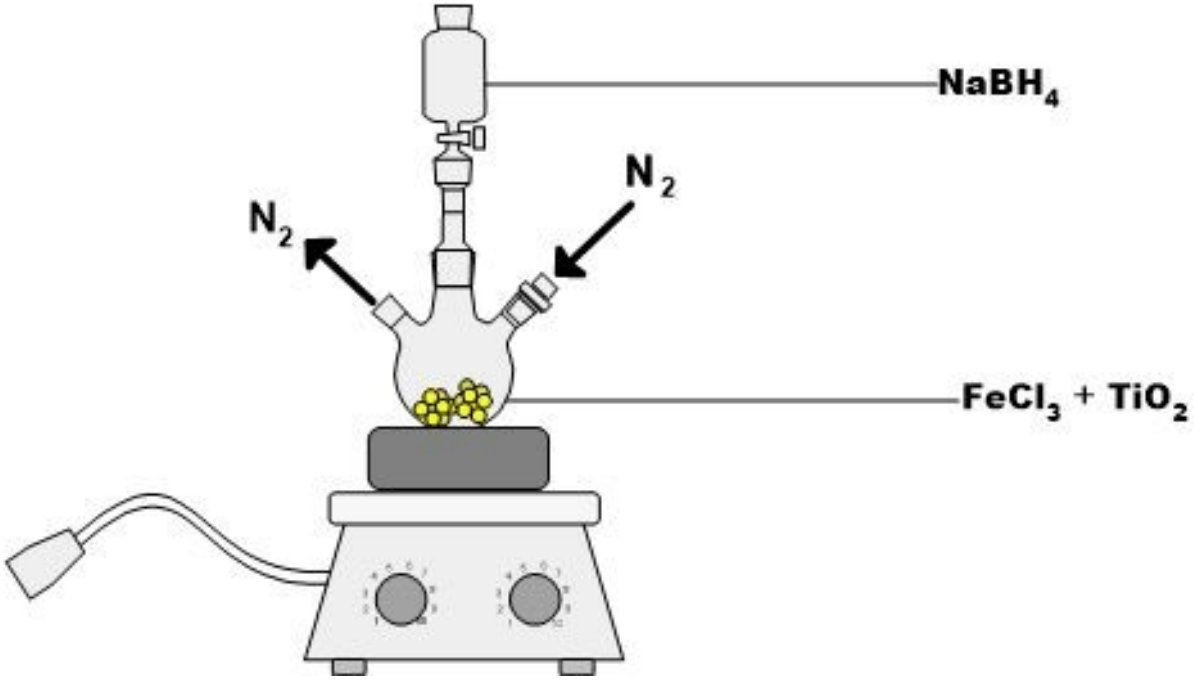

Figure 11. Diagram of experimental setup during the synthesis of zero valent nano iron-doped TiO_2.

3.3. Application Method for the Synthesized Titanium (IV) Oxide Nanoparticle

The photocatalytic properties of reference titanium oxide (T_R) and the synthesized titanium oxide (T_D) were eValuated by the decoloration of orange II sodium salt under a solar light simulator. The source of visible light set-up included an ultra-high efficiency solar simulator equipment (Sciencetech class AAA uhe-nl-150, 1450 Global Drive London, Ontario, Canada). A quantity of photocatalyst sample (T_R or T_D) equal to 5 mg was added to a prepared 10 mg/L orange II sodium (pH 6). The sample was mixed (vortex mixer) and kept in the dark for 5 min. A portion of the prepared sample was subsequently transferred into 1.5 mL cuvette and subsequently subjected to decoloration under the solar simulator for 20 min. The dosage of TiO_2 nanoparticles (T_R or T_D) were varied (50 mg/L, 100 mg/L, 250 mg/L, and 500 mg/L) to obtain an optimum amount. The optimum medium pH was also determined by applying the T_R or T_D (at 250 mg/L been the optimum) at a varied orange II sodium dye solution pH (pH 2, 4, 7, 10 and 11). A control experiment (K) was equally set up (at pH 6) and kept in the dark cupboard for 20 min.

The decoloration of orange II sodium salt (10 mg/L) was monitored with the aid of a PerkinElmer lambda 25 spectrophotometer (absorption measurement). The calculation of the initial (C_0) and final (C) concentration of orange II sodium salt was derived through the absorbance calibration curve. The % decoloration of orange II was calculated as presented in Equation (3)

$$\% \, decolouration = \frac{(C_0 - C)x\ 100}{C_0} \tag{3}$$

3.4. Sample Characterization

Information on structure and crystallite size of the synthesized TiO_2 was obtained with the aid of an X-ray diffractometer (Schimadzu model: XRD 6000) operated with CuKα radiation in the range of 20–80° (λ = 0.154 nm). The functionalization of the TiO_2 was determined using an attenuated total reflectance Nicolet 380 FTIR spectrometer (Thermo Scientific, Waltham, MA, USA). The FTIR spectra were collected in the 500–4000 cm^{-1} range, with a resolution of 4 cm^{-1} at room temperature. Characteristic surface morphologies in TiO_2 nanoparticle were measured with a high resolution scanning electron microscope (Hitachi S4160, Cold Field Emission, voltage 20 KV, Europark, Fichtenhain

A12, 47807 Krefeld, Germany). Meanwhile, Energy-dispersive X-ray (EDX, voltage 20 KV, Take off angle 35.0°) was also applied for the identification of the constituent chemicals in nanoparticles using the SEM instrument. The effect of doping with zero valent nano iron on the surface functionalities and porosities of TiO_2 was investigated by using the nitrogen absorptions as applied in the Quantachrome Brunauer–Emmett–Teller Instrument, Old Pretoria Road Midrand, South Africa (adsorption-desorption isotherm at 77 K, degassing at 150°).

3.5. Computational Simulation

The protocol available in the literature was used for the execution of the computation [45]. The impact of nZVI on the TiO_2 was estimated in terms of variation in the band structure and partial density of states (PDOS) which were computed using the density functional theory (DFT) algorithm in the Cambridge Serial Total Energy Package [46], available in the Material Studio 2019 (Centre for High Performance Computing, Cape Town, South Africa). The general gradient approximation (GGA) exchange–correlational function available in the DFT protocols of the CASTEP was used and the Perdew-Burke-Ernzerhof (PBE) scheme was included. In the primary step, the geometry optimization was performed using Broyden-Fletcher-Goldfarb-Shanno (BFGS) algorithm with convergence of energy change per atom set at 5×10^{-6} eV with stress of 0.02 GPa, displacement of atoms at 0.0005 Å, as well as residual force at 0.01 eV/Å. During the optimization, the FFT (Fast Fourier Transformation) grid was set at $25 \times 25 \times 64$, with $4 \times 4 \times 2$ k-point. The ultrasoft pseudo-potential was applied and the kinetic energy cutoff for the plane-waves basis was 381 eV.

4. Conclusions

A simple reduction process was employed for the novel synthesis of oxygen deficient TiO_2. The excess electrons in nano zero valent iron enabled the creation of an artificial oxygen defect on TiO_2 surface which led to the formation of tetragonal anatase phase solar active TiO_2. There is an enhancement in the photocatalytic properties of the resulting nanoparticles due to their higher absorption in the visible solar spectrum, reduced crystalline sizes and lower energy band gap. The synthesized photo-catalyst also showed optimum activity in the acidic solution of orange II sodium salt. The treatment of contaminated water can be achieved under solar irradiation using the TiO_2, as currently synthesized.

Author Contributions: Conceptualization: K.O.B.; Methodology: F.W.; Software: M.S.; Validation: M.A.-A.; Formal analysis: L.F.P.; Investigation: M.A.-A.; Resources: M.S.; Data curation: M.A.-A.; Writing: Original draft preparation: K.O.B.; Writing—review and editing: K.O.B.; Visualization: L.F.P.; Supervision: F.W. All authors have read and agreed to the published version of the manuscript.

Funding: This research received no external funding.

Acknowledgments: Appreciation to Stefan Maier for hosting me at the department of Physics, Ludwig Maximilians University, Munich, Germany and Namvar Jahanmehr (of the same institution) for his contribution in the analysis (SEM) of the synthesized zero valent nano iron doped TiO_2.

Conflicts of Interest: The authors declare no conflict of interest.

References

1. Khan, M.M.; Adil, S.; Al-Mayouf, A. Metal oxides as photocatalysts. *J. Saudi Chem. Soc.* **2015**, *19*, 462–464. [CrossRef]
2. Ibrahim, M.M.; Mezni, A.; El-Sheshtawy, H.S.; Abu Zaid, A.A.; Alsawat, M.; El-Shafi, N.; Ahmed, S.I.; Shaltout, A.A.; Amin, M.A.; Kumeria, T.; et al. Direct Z-scheme of Cu_2O/TiO_2 enhanced self-cleaning, antibacterial activity, and UV protection of cotton fiber under sunlight. *Appl. Surf. Sci.* **2019**, *479*, 953–962. [CrossRef]
3. Aguirre, M.E.; Zhou, R.; Eugene, A.J.; Guzman, M.I.; Grela, M.A. Cu_2O/TiO_2 heterostructures for CO_2 reduction through a direct Z-scheme: Protecting Cu_2O from photocorrosion. *Appl. Catal. B Environ.* **2017**, *217*, 485–493. [CrossRef]
4. Mestre, A.S.; Carvalho, A.P. Photocatalytic Degradation of Pharmaceuticals Carbamazepine, Diclofenac, and Sulfamethoxazole by Semiconductor and Carbon Materials: A Review. *Molecules* **2019**, *24*, 3702. [CrossRef]

5. Zangeneh, H.; Zinatizadeh, A.; Habibi, M.; Akia, M.; Isa, M.H. Photocatalytic oxidation of organic dyes and pollutants in wastewater using different modified titanium dioxides: A comparative review. *J. Ind. Eng. Chem.* **2015**, *26*, 1–36. [CrossRef]
6. Máynez-Navarro, O.D.; Sánchez-Salas, J.L. Focus on Zinc Oxide as a Photocatalytic Material for Water Treatment. *Int. J. Bioremediation Biodegrad.* **2018**, *2017*, 1–9. [CrossRef]
7. Minero, C.; Vione, D. A quantitative eValution of the photocatalytic performance of TiO_2 slurries. *Appl. Catal. B Environ.* **2006**, *67*, 257–269. [CrossRef]
8. Lee, S.-Y.; Park, S.-J. TiO_2 photocatalyst for water treatment applications. *J. Ind. Eng. Chem.* **2013**, *19*, 1761–1769. [CrossRef]
9. Phuong, N.M.; Chu, N.C.; Van Thuan, D.; Ha, M.N.; Hanh, N.T.; Viet, H.D.T.; Thu, N.T.M.; Van Quan, P.; Truc, N.T.T. Novel Removal of Diazinon Pesticide by Adsorption and Photocatalytic Degradation of Visible Light-Driven Fe-TiO_2/Bent-Fe Photocatalyst. *J. Chem.* **2019**, *2019*, 1–7. [CrossRef]
10. Rehman, S.; Ullah, R.; Butt, A.; Gohar, N. Strategies of making TiO_2 and ZnO visible light active. *J. Hazard. Mater.* **2009**, *170*, 560–569. [CrossRef] [PubMed]
11. Pereira, L.D.O.; Sales, I.M.; Zampiere, L.P.; Vieira, S.S.; Guimarães, I.D.R.; Magalhães, F. Preparation of magnetic photocatalysts from TiO_2, activated carbon and iron nitrate for environmental remediation. *J. Photochem. Photobiol. A Chem.* **2019**, *382*, 111907. [CrossRef]
12. Park, G.D.; Lee, J.; Piao, Y.; Kang, Y.C. Mesoporous graphitic carbon-TiO_2 composite microspheres produced by a pilot-scale spray-drying process as an efficient sulfur host material for Li-S batteries. *Chem. Eng. J.* **2018**, *335*, 600–611. [CrossRef]
13. Nakamura, I.; Negishi, N.; Kutsuna, S.; Ihara, T.; Sugihara, S.; Takeuchi, K. Role of oxygen vacancy in the plasma-treated TiO_2 photocatalyst with visible light activity for NO removal. *J. Mol. Catal. A Chem.* **2000**, *161*, 205–212. [CrossRef]
14. Bethi, B.; Sonawane, S.; Rohit, G.; Holkar, C.; Pinjari, D.; Bhanvase, B.; Pandit, A. Investigation of TiO_2 photocatalyst performance for decolorization in the presence of hydrodynamic cavitation as hybrid AOP. *Ultrason. Sonochem.* **2016**, *28*, 150–160. [CrossRef] [PubMed]
15. Zhang, Z.; Wu, Q.; Johnson, G.; Ye, Y.; Li, X.; Li, N.; Cui, M.; Lee, J.D.; Liu, C.; Zhao, S.; et al. Generalized Synthetic Strategy for Transition-Metal-Doped Brookite-Phase TiO_2 Nanorods. *J. Am. Chem. Soc.* **2019**, *141*, 16548–16552. [CrossRef] [PubMed]
16. Bhatia, V.; Dhir, A. Transition metal doped TiO_2 mediated photocatalytic degradation of anti-inflammatory drug under solar irradiations. *J. Environ. Chem. Eng.* **2016**, *4*, 1267–1273. [CrossRef]
17. Zhang, J.; Fu, D.; Wang, S.; Hao, R.; Xie, Y. Photocatalytic removal of chromium(VI) and sulfite using transition metal (Cu, Fe, Zn) doped TiO_2 driven by visible light: Feasibility, mechanism and kinetics. *J. Ind. Eng. Chem.* **2019**, *80*, 23–32. [CrossRef]
18. Liu, Q.-F.; Zhang, Q.; Liu, B.-R.; Li, S.; Ma, J.-J. Building surface defects by doping with transition metal on ultrafine TiO_2 to enhance the photocatalytic H_2 production activity. *Chin. J. Catal.* **2018**, *39*, 542–548. [CrossRef]
19. Bhardwaj, S.; Pal, B. Effect of variable oxidation states of Mn^{+n} ion impregnated TiO_2 nanocomposites for superior adsorption and photoactivity under visible light. *J. Alloys Compd.* **2020**, *816*, 152639. [CrossRef]
20. Kuo, C.-Y.; Jheng, H.-K.; Syu, S.-E. Effect of non-metal doping on the photocatalytic activity of titanium dioxide on the photodegradation of aqueous bisphenol A. *Environ. Technol.* **2019**, *42*, 1603–1611. [CrossRef]
21. Mouele, E.S.M.; Dinu, M.; Cummings, F.; Fatoba, O.O.; Myint, M.T.Z.; Kyaw, H.H.; Parau, A.C.; Vladescu, A.; Francesconi, M.G.; Pescetelli, S.; et al. Effect of Calcination Time on the Physicochemical Properties and Photocatalytic Performance of Carbon and Nitrogen Co-Doped TiO_2 Nanoparticles. *Catalysts* **2020**, *10*, 847. [CrossRef]
22. Basavarajappa, P.S.; Patil, S.B.; Ganganagappa, N.; Reddy, K.R.; Raghu, A.V.; Reddy, C.V. Recent progress in metal-doped TiO_2, non-metal doped/codoped TiO_2 and TiO_2 nanostructured hybrids for enhanced photocatalysis. *Int. J. Hydrogen Energy* **2020**, *45*, 7764–7778. [CrossRef]
23. Danilov, F.I.; Tsurkan, A.; Vasil'Eva, E.; Protsenko, V. Electrocatalytic activity of composite Fe/TiO_2 electrodeposits for hydrogen eVolution reaction in alkaline solutions. *Int. J. Hydrog. Energy* **2016**, *41*, 7363–7372. [CrossRef]
24. Badmus, K.O.; Coetsee-Hugo, E.; Swart, H.; Petrik, L. Synthesis and characterisation of stable and efficient nano zero valent iron. *Environ. Sci. Pollut. Res.* **2018**, *25*, 23667–23684. [CrossRef]
25. Sotoudeh, M.; Abbasnejad, M.; Mohammadizadeh, M.R. First principles study of hydrogen doping in anatase TiO_2. *Eur. Phys. J. Appl. Phys.* **2014**, *67*, 30401. [CrossRef]
26. Hsu, C.-L.; Wu, H.-Y.; Fang, C.-C.; Chang, S.-P. Solution-Processed UV and Visible Photodetectors Based on Y-Doped ZnO Nanowires with TiO_2 Nanosheets and Au Nanoparticles. *ACS Appl. Energy Mater.* **2018**, *1*, 2087–2095. [CrossRef]
27. Reinosa, J.J.; Docio, C.M.Á.; Ramírez, V.Z.; Lozano, J.F.F. Hierarchical nano ZnO-micro TiO_2 composites: High UV protection yield lowering photodegradation in sunscreens. *Ceram. Int.* **2018**, *44*, 2827–2834. [CrossRef]
28. Kang, X.; Liu, S.; Dai, Z.; He, Y.; Song, X.; Tan, Z. Titanium Dioxide: From Engineering to Applications. *Catalysts* **2019**, *9*, 191. [CrossRef]
29. He, X.; Tang, A.; Yang, H.; Ouyang, J. Synthesis and catalytic activity of doped TiO_2-palygorskite composites. *Appl. Clay Sci.* **2011**, *53*, 80–84. [CrossRef]
30. Hejri, Z.; Hejri, M.; Omidvar, M.; Morshedi, S. Synthesis of TiO_2/nZVI nanocomposite for nitrate removal from aqueous solution. *Int. J. Ind. Chem.* **2019**, *10*, 225–236. [CrossRef]
31. El Mragui, A.; Logvina, Y.; Da Silva, L.P.; Zegaoui, O.; Da Silva, J.C.E. Synthesis of Fe- and Co-Doped TiO_2 with Improved Photocatalytic Activity Under Visible Irradiation Toward Carbamazepine Degradation. *Materials* **2019**, *12*, 3874. [CrossRef] [PubMed]

32. Nosaka, Y.; Nosaka, A. Understanding Hydroxyl Radical (•OH) Generation Processes in Photocatalysis. *ACS Energy Lett.* **2016**, *1*, 356–359. [CrossRef]
33. An, H.-R.; Hong, Y.C.; Kim, H.; Huh, J.Y.; Park, E.C.; Park, S.Y.; Jeong, Y.; Park, J.-I.; Kim, J.-P.; Lee, Y.-C.; et al. Studies on mass production and highly solar light photocatalytic properties of gray hydrogenated-TiO_2 sphere photocatalysts. *J. Hazard. Mater.* **2018**, *358*, 222–233. [CrossRef] [PubMed]
34. Yu, X.; Kim, B.; Kim, Y.K. Highly Enhanced Photoactivity of Anatase TiO_2 Nanocrystals by Controlled Hydrogenation-Induced Surface Defects. *ACS Catal.* **2013**, *3*, 2479–2486. [CrossRef]
35. Xu, J.; Li, L.; Yan, Y.; Wang, H.; Wang, X.; Fu, X.; Li, G. Synthesis and photoluminescence of well-dispersible anatase TiO_2 nanoparticles. *J. Colloid Interface Sci.* **2008**, *318*, 29–34. [CrossRef] [PubMed]
36. Haider, A.J.; Anbari, R.H.A.; Kadhim, G.R.; Salame, C.T. Exploring potential Environmental applications of TiO_2 Nanoparticles. *Energy Procedia* **2017**, *119*, 332–345. [CrossRef]
37. Chang, J.; Zhang, Q.; Liu, Y.; Shi, Y.; Qin, Z. Preparation of Fe_3O_4/TiO_2 magnetic photocatalyst for photocatalytic degradation of phenol. *J. Mater. Sci. Mater. Electron.* **2018**, *29*, 8258–8266. [CrossRef]
38. Petala, E.; Baikousi, M.; Karakassides, M.A.; Zoppellaro, G.; Filip, J.; Tuček, J.; Vasilopoulos, K.C.; Pechoušek, J.; Zbořil, R. Synthesis, physical properties and application of the zero-valent iron/titanium dioxide heterocomposite having high activity for the sustainable photocatalytic removal of hexavalent chromium in water. *Phys. Chem. Chem. Phys.* **2016**, *18*, 10637–10646. [CrossRef]
39. Yun, D.-M.; Cho, H.-H.; Jang, J.-W.; Park, J.-W. Nano zero-valent iron impregnated on titanium dioxide nanotube array film for both oxidation and reduction of methyl orange. *Water Res.* **2013**, *47*, 1858–1866. [CrossRef]
40. Yan, J.; Wu, G.; Guan, N.; Li, L.; Li, Z.; Cao, X. Understanding the effect of surface/bulk defects on the photocatalytic activity of TiO_2: Anatase versus rutile. *Phys. Chem. Chem. Phys.* **2013**, *15*, 10978–10988. [CrossRef]
41. Hengerer, R.; Bolliger, B.; Erbudak, M.; Grätzel, M. Structure and stability of the anatase TiO_2 (101) and (001) surfaces. *Surf. Sci.* **2000**, *460*, 162–169. [CrossRef]
42. Zhao, H.; Pan, F.; Li, Y. A review on the effects of TiO_2 surface point defects on CO_2 photoreduction with H_2O. *J. Mater.* **2017**, *3*, 17–32. [CrossRef]
43. Li, H.; Guo, Y.; Robertson, J. Calculation of TiO_2 Surface and Subsurface Oxygen Vacancy by the Screened Exchange Functional. *J. Phys. Chem. C* **2015**, *119*, 18160–18166. [CrossRef]
44. Sarvari, N.; Mohammadi, M.R. Influence of photoanode architecture on light scattering mechanism and device performance of dye-sensitized solar cells using TiO_2 hollow cubes and nanoparticles. *J. Taiwan Inst. Chem. Eng.* **2018**, *86*, 81–91. [CrossRef]
45. Luo, X.; Zhu, S.; Wang, J.; Wang, C.; Wu, M. Characterization and Computation of Yb/TiO_2 and Its Photocatalytic Degradation with Benzohydroxamic Acid. *Int. J. Environ. Res. Public Health* **2017**, *14*, 1471. [CrossRef] [PubMed]
46. Clark, S.J.; Segall, M.D.; Pickard, C.J.; Hasnip, P.J.; Probert, M.J.; Refson, K.; Payne, M.C. First principles methods using CASTEP. *Z. Krist.* **2005**, *220*, 567–570. [CrossRef]